



Effects of Space Environment on Flow and Concentration During Directional Solidification

C. Benjapiyaporn, V. Timchenko, E. Leonardi and G. de Vahl Davis
The University of New South Wales, Sydney NSW, Australia

H.C. de Groh III
Glenn Research Center, Cleveland, Ohio

National Aeronautics and
Space Administration

Glenn Research Center

Acknowledgments

The UNSW authors acknowledge with thanks the support of the Australian Research Council and the Australian Department of Industry, Science and Technology. The authors wish to thank and acknowledge Prof. Reza Abbaschian of the University of Florida at Gainesville who is the Principal Investigator of the Space Shuttle Flight Experiment MEPHISTO-2 and -4. Our collaboration with him on MEPHISTO formed the foundation and starting point for this work.

Trade names or manufacturers' names are used in this report for identification only. This usage does not constitute an official endorsement, either expressed or implied, by the National Aeronautics and Space Administration.

Available from

NASA Center for Aerospace Information
7121 Standard Drive
Hanover, MD 21076
Price Code: A03

National Technical Information Service
5285 Port Royal Road
Springfield, VA 22100
Price Code: A03

Available electronically at <http://gltrs.grc.nasa.gov/GLTRS>

EFFECTS OF SPACE ENVIRONMENT ON FLOW AND CONCENTRATION DURING DIRECTIONAL SOLIDIFICATION

C. Benjapiyaporn, V. Timchenko, E. Leonardi and G. de Vahl Davis
The University of New South Wales, Sydney NSW, Australia

H. C. de Groh III
NASA Glenn Research Center, Cleveland OH, USA

AN IMPORTANT FORWARD

This paper was designed to be viewed on the World Wide Web using a computer with an internet browser such as Netscape¹ or Microsoft Internet Explorer.¹ Key information in the web based version is presented in the form of nine animated movies. These movies are not present in this paper copy. It is hoped that this paper (and thus the movies) can be easily viewed by accessing the following URL:

<ftp://ftp-gltrs.grc.nasa.gov/GLTRS/reports/2000/TM-2000-209293/index.html>

It is also expected that a link to the full paper will be present on the web page of de Groh whose home page is at the URL address: <http://cml.lerc.nasa.gov/degroh>

This paper was published in the International Journal of Fluid Dynamics (2000), Vol.4, Article 3; which is an internet publication. Thus, at the time of this printing, the paper can also be accessed via the URL:

http://sibley.mae.cornell.edu/IJFD/2000_vol4/paper3/index.html

ABSTRACT

A study of directional solidification of a weak binary alloy (specifically, Bi – 1 at% Sn) based on the fixed grid single domain approach is being undertaken. The enthalpy method is used to solve for the temperature field over the computational domain including both the solid and liquid phases; latent heat evolution is treated with the aid of an effective specific heat coefficient. A source term accounting for the release of solute into the liquid during solidification has been incorporated into the solute transport equation. The vorticity-stream function formulation is used to describe thermo-solutal convection in the liquid region.

In this paper we numerically investigate the effects of g-jitter on directional solidification. A background gravity of 1 μg has been assumed, and new results for the effects of periodic disturbances over a range of amplitudes and frequencies on solute field and segregation have been presented.

¹ Any trade names, registered trade marks, or products mentioned in this paper are done so for completeness only; no endorsement of any product should be inferred.

1. INTRODUCTION

The investigation of solidification and melting processes in low gravity conditions is of great practical importance for crystal growth techniques. The quality of single crystals grown from the melt strongly depends on growth morphology and macro-segregation caused by convective heat and mass transfer effects. A low gravity environment produces conditions in which convection is decreased to a level at which crystal growth is largely diffusion controlled. Residual accelerations in orbiting space vehicles are of the order of one to several thousand μg (where $1 \mu g = 9.81 \times 10^{-6} \text{ ms}^{-2}$). To achieve diffusion dominated conditions, much effort has been expended in recent years in performing crystal growth experiments in the microgravity environment of a spacecraft in earth orbit⁷⁻¹². Such effects as constitutional and kinetic supercooling, and the influence of convection on solute distribution in the melt, have been investigated under microgravity.

However, gravity in an orbiting space vehicle may not be steady in either magnitude or direction. Perturbations to the anticipated steady microgravity environment may arise from, for example, crew actions, the operation of machinery and thruster rocket firings. Such perturbations are known as g-jitter.^{1,2,13-16}

The effects of gravity perturbations on composition distribution in the Bridgman crystal growth configuration have been investigated numerically in a number of papers. Alexander, Ouazzani and Rosenberger¹ investigated the effects of steady and impulse residual acceleration on dopant distribution in Bridgman-Stockbarger crystal growth with different gravity vector orientations. It was found that lateral non-uniformity in composition is very sensitive to the orientation of the steady component of the residual gravity vector.

Transient and periodic accelerations have been considered in Alexander, Amiroudine, Ouazzani, and Rosenberger². It was found that the largest compositional nonuniformities occur for disturbances with amplitudes above $10^{-6}g$ and frequencies below 10^{-2} Hz . At higher frequencies, larger acceleration amplitudes are required to obtain significant nonuniformities. Numerical results for the effect of g-jitter on the average interface concentration during Bridgman crystal growth in space are presented in Garandet, Corre, Favier and Alexander³. In all of these works a pseudo-steady-state model was adopted with the constraint that the interface is planar. This is a simplification of the true unsteady solidification process.

In actual growth situations the solid-liquid interface can be non-planar due to thermal and mass transfer conditions and also due to morphological instability factors. Pseudo-steady-state models neglect transient effects such as changes in the interface velocity, temperature and concentration with time due to changes in the length of melt caused by the finite length of the ampoule. Investigation of solute redistribution during the initial transients becomes crucial for an alloy with a low partition coefficient solidifying at low rates because the length of the initial transient is very long, thus steady state is difficult to reach.

In this work we investigate effects of periodic gravity perturbations on segregation and solute distribution during transient directional solidification of Bi-1 at % Sn alloy in a Bridgman furnace. A background gravity of $1 \mu g$, which corresponds to a typical spacecraft environment, is considered. The influence of solute on liquid density is included. The interface is assumed to be at the melting temperature of pure Bi. The diffusion coefficient for Sn in Bi is assumed to be constant. The general boundary conditions used are similar to NASA's MEPHISTO-2 and -4 Shuttle Flight experiments.

2. MATHEMATICAL FORMULATION

We consider a Bridgman furnace in which a moving temperature profile consisting of a cold zone (T_c), a nominally adiabatic zone and a hot zone (T_h) is imposed on the boundary of the ampoule. This boundary temperature profile is translated with a constant pulling velocity, as a result of the furnace movement, causing the solid/liquid interface to move along the ampoule. The material in the ampoule is thus divided into two regions: solid and liquid.

Although the ampoule is three-dimensional, a two-dimensional model is used. This simplification is valid because, under the microgravity conditions being considered, convection is very weak and the solidification process remains largely diffusion-controlled and the flow that does arise is predominantly 2-D in nature. Newtonian and laminar flow is assumed in the liquid phase, and the Boussinesq approximation has been used, in which the liquid density is assumed to be constant except in the buoyancy term of the equation of motion.

The governing time dependant equations describing mass, momentum, heat and solute transport in a vorticity-stream function formulation are:

$$\rho \left(\frac{\partial \zeta}{\partial t} + \nabla \cdot (\tilde{v} \zeta) \right) = \nabla \rho \times \hat{g} |g| + \mu \nabla^2 \zeta \quad (1)$$

$$\nabla^2 \psi = -\zeta \quad (2)$$

$$\rho c_p \left(\frac{\partial T}{\partial t} + \nabla \cdot (\tilde{v} T) \right) = \lambda \nabla^2 T \quad (3)$$

$$\frac{\partial C}{\partial t} + \nabla \cdot (\tilde{v} C) = D \nabla^2 C \quad (4)$$

where t , ρ , μ , c_p , λ and D are respectively the time, density, viscosity, specific heat and thermal conductivity of the alloy and the diffusivity of the solute; ζ , ψ , T , \tilde{v} and C are respectively the vorticity, stream function, temperature, velocity vector and solute concentration; g is the magnitude of the gravitational acceleration, and \hat{g} is the unit vector in the direction of gravity. The density in the buoyancy term of equation (1) is assumed to be a linear function of temperature and solute concentration:

$$\rho = \rho_R [1 - \beta_T (T - T_R) + \beta_C (C - C_R)] \quad (5)$$

where β_T and β_C are the thermal and solutal expansion coefficients,

$$\beta_T = -\frac{1}{\rho_R} \frac{\partial \rho}{\partial T} \quad (6)$$

and

$$\beta_C = \frac{1}{\rho_R} \frac{\partial \rho}{\partial C} \quad (7)$$

ρ_R , T_R and C_R are the reference density, temperature and concentration.

The gravitational acceleration is taken as:

$$g(t) = g_0 + A \sin(2\pi\omega t) \quad (8)$$

where A is the amplitude of the acceleration, ω is the frequency and g_0 is the steady component of the acceleration.

Enthalpy method

To model the process of directional solidification we have chosen the enthalpy method⁴ which avoids explicit tracking of the solid/liquid interface.

Latent heat evolution during phase change is incorporated in the energy equation using the following definition of enthalpy. For each phase ϕ , enthalpy is defined as

$$h = \int_0^T c_{p\phi} dT + f_l L, \quad (9)$$

where L is latent heat and f_l is the local liquid volume fraction.

For isothermal phase change the liquid fraction is determined by the melting temperature T_m :

$$\begin{aligned} \text{for } T > T_m \quad f_l &= 1 \\ \text{for } T < T_m \quad f_l &= 0. \end{aligned} \quad (10)$$

With the assumption that specific heat $c_{p\phi}$ is constant in each phase, (9) can be written as

$$h = c_{p\phi} T + f_l L = h_{sens} + f_l L. \quad (11)$$

Here h_{sens} is the sensible heat, and the subscripts l and s refer to the liquid and solid phases.

Using the apparent heat capacity method⁵, an effective specific heat can be defined by

$$C^*(T) = \frac{\partial h}{\partial T} = c_{p\phi} + L \frac{\partial f_l}{\partial T}. \quad (12)$$

Using (12), the energy equation (3) can be written:

$$\rho [C^*(T) \frac{\partial T}{\partial t} + c_{p\phi} \nabla \cdot (\vec{v} T)] = \lambda \nabla^2 T. \quad (13)$$

To solve equation (13), an effective heat capacity coefficient $\partial f_l / \partial T$ has to be calculated. We define

$$\frac{\partial f_l}{\partial T} = \frac{\partial f_l / \partial n}{\partial T / \partial n} = \frac{(f_l)_n T_n}{T_n^2} = \frac{(f_l)_x T_x + (f_l)_y T_y}{T_x^2 + T_y^2} \quad (14)$$

where the subscripts n (denoting the normal direction), x and y denote differentiation.

Since isothermal phase change is under consideration, the liquid fraction undergoes a step change when the interface crosses a grid line. This abrupt change in the liquid fraction, defined by the step function (10), can cause serious numerical instabilities. To overcome this problem, a control volume was defined around each grid point, in which the liquid fraction could be estimated. Phase change was considered to take place over one control volume, in which the step function (10) is replaced by a linear approximation:

$$\begin{aligned} \text{for } T_{ij} > T_m + \Delta T \quad f_l &= 1 \\ \text{for } T_m - \Delta T \leq T_{ij} \leq T_m + \Delta T \quad f_l &= \frac{T_{ij} - T_m + \Delta T}{2\Delta T} \\ \text{for } T_{ij} < T_m - \Delta T \quad f_l &= 0 \end{aligned} \quad (15)$$

where $2\Delta T$ is a temperature interval chosen to represent the range over which phase change occurs in the (i, j) control volume.

Based on the calculated values of liquid fraction at each mesh point the computational domain was subdivided into sub-regions of solid and liquid phases.

In the solid, the vorticity, stream function and velocities were set to zero. In the liquid, they are calculated from the stream function defined as:

$$\tilde{v} = \nabla \times \tilde{\psi} \quad (16)$$

Solute transport with phase change

The release of solute into the liquid during solidification can be described by considering an average concentration in an arbitrary control volume which is undergoing phase change⁴. This control volume can be treated as partially solidified with an average concentration defined as:

$$C = f_s C_s + f_l C_l \quad (17)$$

where $f_s = 1 - f_l$ is the local solid volume fraction. Since diffusion in the solid is neglected, the concentration in the solid remains constant over time. Noting that $C_s = kC_l$ we can thus write:

$$\frac{\partial C}{\partial t} = -\frac{\partial f_l}{\partial t}(1-k)C_l + (1-f_l)\frac{\partial C_l}{\partial t} \quad (18)$$

When (18) is used in the solute transport equation (4), we obtain the solute conservation equation in the form:

$$\frac{\partial C_l}{\partial t} + \nabla \cdot (\tilde{v} C_l) = D \nabla^2 C_l + S_c \quad (19)$$

in which

$$S_c = \frac{\partial f_l}{\partial t}(1-k)C_l + f_l \frac{\partial C_l}{\partial t} \quad (20)$$

The formulation for solute transport during phase change described by equations (19) and (20) allows for the solution for liquid concentration only and hence bypasses the concentration discontinuity at the interface.

3. NUMERICAL METHOD

An algorithm entitled SOLCON⁶, which incorporates the closely coupled solution of the transport equations in the vorticity-stream function formulation, was used. To ensure stability of the computational process, all source terms and non-linear coefficients depending on liquid fraction are linearized based on the value of liquid fraction obtained from the previous iteration.

The vorticity, stream function and energy equations were discretized using central differences and solved by a modified ADI scheme with internal iterations. Interface boundary conditions for vorticity and stream function were applied at those mesh points in the solid sub-region which are adjacent to the liquid. For the calculation of vorticity boundary conditions, the definition of vorticity was used:

$\tilde{\zeta} = \nabla \times \tilde{v}$. The boundary condition $\psi = 0$ was used for the stream function. The concentration equation (19) was discretized and solved using a control volume approach. This ensures mass balance during phase change in the partially solidified control volume. A second order upwind scheme (SOU) was used for the convection fluxes with central differences for the diffusion terms.

To account for the fact that the computed concentration is a cell average value, an exponential extrapolation procedure based on the liquid fraction has been introduced to find the values of the concentration at the solid/liquid interface. The liquid side interface solute concentration C_l can then be used to determine the concentration in the solid as it forms.

4. CODE VALIDATION

To validate the code, computations were performed for directional solidification of gallium-doped germanium crystal grown by the Bridgman-Stockbarger technique as described by Alexander *et al.*². Comparisons were made for the case of sinusoidal acceleration with an amplitude of $10^{-3}g$ and a frequency of 10^{-1} Hz oriented parallel to the solid-liquid interface.

In Alexander *et al.*² a pseudo-steady model was adopted with the assumption that the ampoule translation rate and the growth rate are equal. In their model the solid-liquid interface is located at a fixed distance from the top of computational domain, which is completely occupied by the melt. The aspect ratio of the computational domain was equal to 1. On the other hand the model used in the current study considers transient effects and hence the gradual decrease in the length of melting zone. Both solid and liquid phases are included in the computational domain (see Figure 1).

The temperature profile is translated with a constant pulling velocity along the boundary causing the interface movement inside the domain. The boundary temperature profile, size of the computational domain and physical properties of the alloy were chosen to approximate the idealized model of the Bridgman-Stockbarger system in Alexander *et al.*². T_c was equal to 1131K and T_h was 1331K. The length of the computational domain was taken to be 21 mm, the height was 10 mm and the adiabatic zone was 5 mm. A uniform square 51 x 106 mesh was used.

A steady solution for the temperature and flow was used as the initial condition for the transient growth. This steady solution was obtained by keeping the boundary temperature profile stationary with the solid-liquid interface located at 7 mm from the left wall of the ampoule. The initial solute concentration in the liquid was uniform at 1 at%. Solidification was first started with a constant gravity level of $1 \mu g$ and when 3 mm of material was solidified, a sinusoidal acceleration with an amplitude of $10^{-3}g$ and frequency of 10^{-1} Hz (oriented parallel to the solid-liquid interface) was imposed for another 2 mm of solidification. The translation velocity was $6.5 \mu m/s$.

Figure 2 shows the maximum vertical velocity as a function of time computed using the present model. The velocity field is in phase with the residual acceleration. This result is in excellent agreement with Figure 7b from Alexander *et al.*².

Table 1. Comparison of the two models.

	U_{max} (mm/s)	V_{max} (mm/s)	$\gamma_{c, max} - \gamma_0$ (%)
Alexander <i>et al.</i> ²	0.1140	0.1325	19.14
Present work	0.1175	0.1338	19.80
% difference	3.07	0.98	3.5

Table 1 shows a quantitative comparison of the results obtained from the two models. U_{max} and V_{max} are the maximum velocity components along and across the ampoule respectively (during one period), and γ_c is the radial segregation at the interface in the liquid defined by

$$\gamma_c = (C_{max} - C_{min}) / C_{ave} \times 100\% \quad (21)$$

where the three values of the concentration are taken in the liquid at the interface and γ_0 is segregation

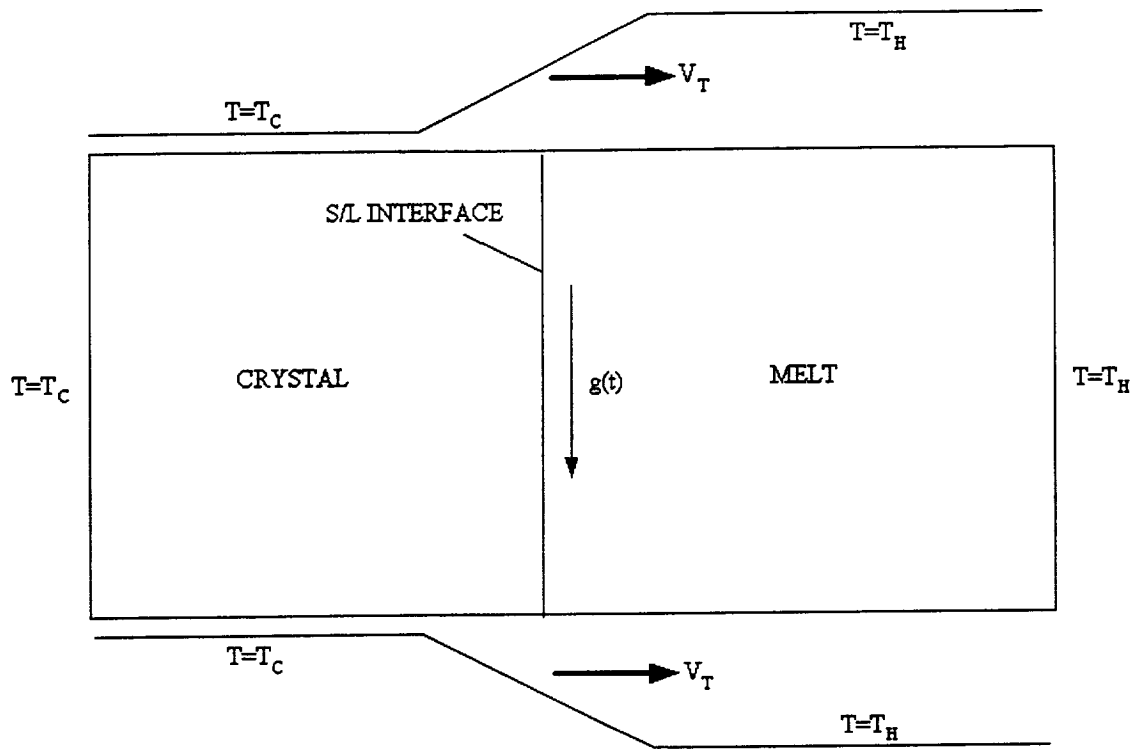


Figure 1. Model used in the present work for comparison with Alexander *et al.*²

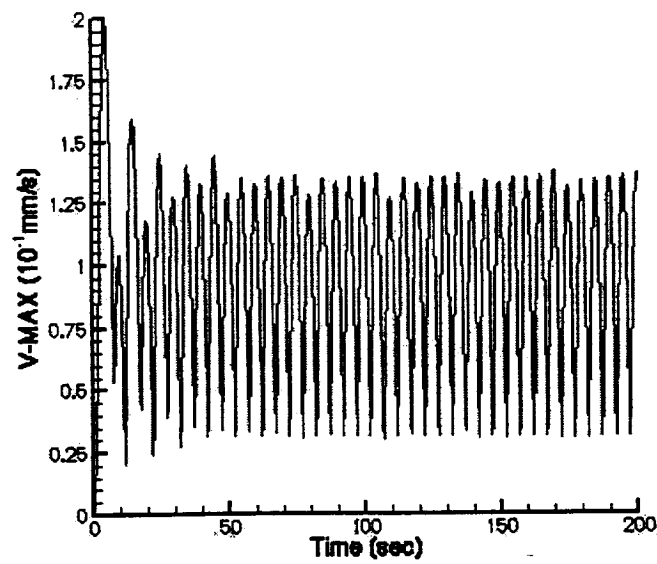


Figure 2. Maximum vertical velocity for a sinusoidal acceleration with an amplitude of $10^{-3}g$ and frequency of 10^{-1} Hz .

before the g-jitter starts. In the case of Alexander *et al.*² γ_0 was equal to zero, in the present calculations the initial segregation was 4.0%.

The maximum change in segregation during g-jitter was equal to 19.14% (Alexander *et al.*²) and 19.8% (our calculations). This was reached after 230 seconds of solidification.

It is obvious that computed results are in very good agreement despite the difference in the physical and mathematical models.

Solidification of Bi-Sn Alloy

Simulations were performed for directional solidification of Bi-1at% Sn alloy in a Bridgman furnace. Property values are taken from Timchenko *et al.*⁶ and shown in the Table 2 below.

Table 2. Property values used in the computations

Property	Symbol	Value
Density	ρ	10,070 kg/m ³
Specific heat	C_p	144.87 J/kg K
Thermal conductivity	λ	12.4 W/m K
Thermal diffusivity	α	8.500×10 ⁻⁶ m ² /s
Kinematic viscosity	ν	1.837×10 ⁻⁷ m ² /s
Diffusion coefficient for Sn in Bi	D	2.7×10 ⁻⁹ m ² /s
Thermal expansion coefficient	β_T	1.25×10 ⁻⁴ K ⁻¹
Solutal expansion coefficient	β_C	-0.305 (kg Sn/kg alloy) ⁻¹
Temperature gradient in adiabatic zone	dT/dx	200 K/cm
Partition coefficient	k	0.029 at%/at%

The domain studied has a height of 6 mm and a length of 42 mm. The boundary temperature profile imposed on the outer surface of the liquid boundary consisted of a cold zone ($T_c = 50^\circ \text{C}$), linear temperature profile with a gradient 20 K/mm (for a length of 32.5 mm) and a hot zone ($T_h = 700^\circ \text{C}$). That is, conduction in the ampoule wall was not considered. The computational domain initially contains only liquid with a uniform solute concentration C_0 of 1 at% and uniform temperature of 700 °C. At the left boundary an initial temperature of 272 °C was imposed. The pulling velocity, the rate of translation of the boundary temperature distribution, was 3.34 $\mu\text{m/s}$, and solidification occurred from left to right as time progressed. These boundary conditions are very similar to those present during the MEPHISTO-2 and -4 Space Flight experiments.^{11,12}

Mesh validation

To ensure the accuracy of the solution a mesh validation was performed for 500 seconds of solidification. The gravity vector was 1 μg , acting in a direction normal to the axis of the ampoule.

Three different mesh sizes were used, with the number of mesh points equal to 31 x 211, 31 x 421 and 61 x 421. The time step used with the 31 x 211 mesh was 0.1 s, and for the 31 x 421 and 61 x 421 meshes it was 0.01 s. The difference between those results is listed in Table 3. The length of the solute boundary layer is about 2 mm (estimated from the diffusion based analytical solution as $2D/R$ and previous numerical solutions⁶) thus the coarsest mesh provides about 10 mesh points within the solute

boundary layer.

Table 3. Mesh validation

	31 x 211	31 x 421	61 x 421
U_{max} mm/s	2.286×10^{-4} (0.7%)	2.286×10^{-4} (0.7%)	2.302×10^{-4} (-)
V_{max} mm/s	1.395×10^{-4} (0.35%)	1.400×10^{-4} (0.0%)	1.400×10^{-4} (-)
C_{max} at%	3.2997 (0.4%)	3.2871 (0.0%)	3.2868 (-)

From Table 3, it can be concluded that a 31 x 211 mesh can be used in the calculations.

5. RESULTS AND DISCUSSION

The effects of periodic disturbances on the compositional profile and segregation at the interface have been investigated. The amplitudes were varied from $10^{-5}g$ to $10^{-2}g$ for a range of frequencies from 10^{-2} to 1 Hz.

At first, computations were performed for solidification with a constant gravity level of $1 \mu g$. After 1500 seconds, sinusoidal accelerations oriented parallel to the solid-liquid interface were imposed and computations with g-jitter were performed for a further 500 seconds.

For comparison purposes, computations with a steady gravity level of $1 \mu g$ were performed. The results of these computations are summarised in [Table 4](#). It can be seen that for a given acceleration magnitude, larger segregation at the interface occurs for smaller frequencies or longer periods of disturbances. The same effect was reported in Alexander *et al.*². Disturbances with amplitudes of $10^{-5}g$ produce very little effect on the segregation or the compositional profile. Disturbances with amplitudes of $10^{-4}g$ cause increases in the segregation from 2.7 to 4.9% (1.8% for steady $1 \mu g$ gravity) when the frequencies of the disturbances become lower than 0.1 Hz. Larger effects on segregation were observed for disturbances with an amplitude of $10^{-3}g$.

[Figure 3](#) shows the vertical velocity at a reference point as a function of time, for frequencies of the disturbances of (a) 0.01 Hz, (b) 0.1 Hz and (c) 1 Hz with an amplitude of $10^{-3}g$. The reference point is moving with the interface and is always located 2 mm in front of the interface at the mid-height of the domain. The development of the velocity field occurs in phase with the gravitational acceleration. The maximum velocity exhibits a transient before reaching steady oscillations. This transient includes number of periods which increases with increasing frequency as can be seen clearly in [Figure 3\(c\)](#). As the frequency is reduced the maximum velocity increases.

Velocity Field

Consider [Movie 1](#), [Movie 2](#) and [Movie 3](#), they show that the configuration of the flow field depends on frequency of the disturbance. The velocity field in these three movies is quite different, especially during the reversal period. For the small frequency of disturbance 0.01 Hz, the reversal period is very small (2-3 seconds), as seen in [Movie 1](#) when the contour colour of stream function changes from red to blue or blue to red. During the reversal period of the 0.1 Hz case, a weak recirculation occurs in front of the interface, as seen in [Movie 2](#) which is not present in the 0.01Hz case. For 1.0 Hz of disturbance, the flow configuration is much different from the previous two cases. At high frequency of disturbance, the flow does not reverse. As seen in [Movie 3](#), the flow is periodically changing from strong clockwise flow to weak clockwise flow. It is also observed that there is a weak recirculation cell in front of the interface.

The velocity field needs time to respond to the acceleration, therefore, a major factor on the velocity field is frequency or the period of the disturbance. For the small frequencies of the disturbance, the velocity field has enough time to develop corresponding to the changing acceleration field. As a result, the maximum velocity in this case is close to that with the steady gravitational field at the peak of the disturbance. In contrast, for high frequencies of the disturbance, the flow field does not have enough time (in one cycle) to develop corresponding to the oscillating part of the acceleration. Therefore, the maximum velocity is close to that with the steady gravitational field at the back ground level, as seen in [Figure 4](#).

Concentration Field

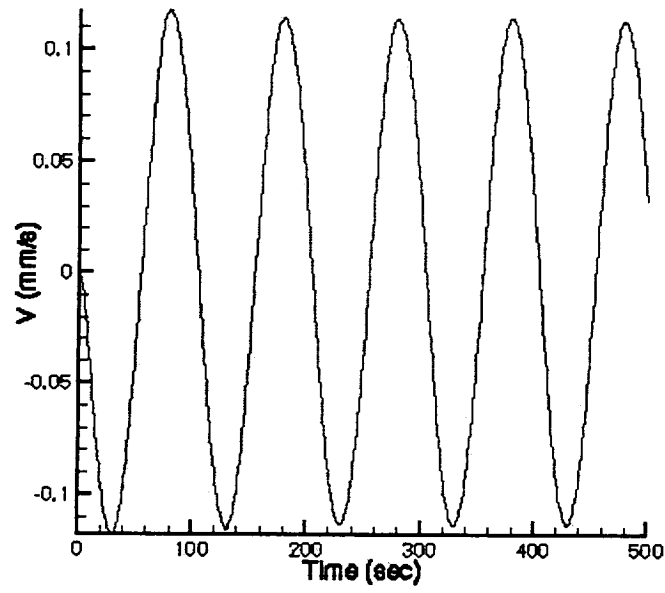
It has been shown from [Table 4](#) that the low frequencies and large amplitudes of the disturbance do have an effect on the segregation of the solute. Therefore, the following movies will demonstrate how the solutal field is responding to the disturbance.

[Movie 4](#) shows the effects of the disturbance of 0.01Hz and $10^{-2}g$. Due to a very strong amplitude and low frequency of the disturbance, strong convection is observed. The flow is strong enough to

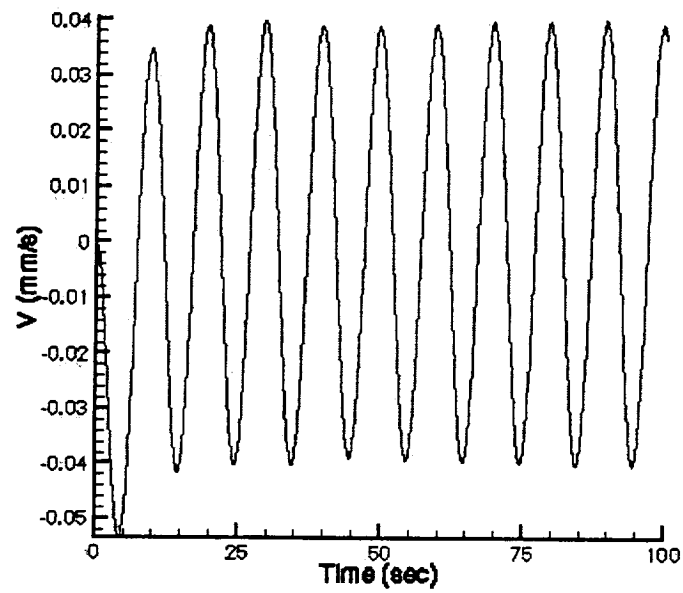
Table 4. Summary of results

Amplitude (m/s ²)	Frequency (Hz)	Maximum velocity (mm/s)		Maximum segregation (%)	Segregation after 500s solidification (with g-jitter) (%)
		U_{max}	V_{max}		
10 ⁻² g	0.01	2.50	0.89	188.7	90.0
	0.05	1.26	0.78	192.4	188.0
	0.1	0.75	0.32	39.9	39.9
	0.5	0.19	9.66x10 ⁻²	20.2	20.2
	1.0	9.78x10 ⁻²	4.81x10 ⁻²	10.9	10.9
10 ⁻³ g	0.01	0.22	0.11	38.2	33.0
	0.05	0.12	6.75x10 ⁻²	11.3	10.3
	0.1	7.49x10 ⁻²	4.13x10 ⁻²	8.9	8.9
	0.5	1.90x10 ⁻²	9.78x10 ⁻³	3.1	3.1
	1.0	9.95x10 ⁻³	4.94x10 ⁻³	2.5	2.5
10 ⁻⁴ g	0.01	2.15x10 ⁻²	1.15x10 ⁻²	4.9	4.3
	0.05	1.27x10 ⁻²	6.86x10 ⁻³	2.7	2.7
	0.1	7.68x10 ⁻³	4.23x10 ⁻³	2.3	2.3
	0.5	2.06x10 ⁻³	1.08x10 ⁻³	1.8	1.8
	1.0	1.14x10 ⁻³	6.02x10 ⁻⁴	1.8	1.8
10 ⁻⁵ g	0.01	2.41x10 ⁻³	1.27x10 ⁻³	2.0	2.0
	0.05	1.47x10 ⁻³	7.96x10 ⁻⁴	1.8	1.8
	0.1	9.66x10 ⁻⁴	5.29x10 ⁻⁴	1.8	1.8
	0.5	3.85x10 ⁻⁴	2.12x10 ⁻⁴	1.8	1.8
	1.0	2.97x10 ⁻⁴	1.65x10 ⁻⁴	1.8	1.8
	steady	2.28x10 ⁻⁴	1.20x10 ⁻⁴	1.8	1.8

Table 4 Velocity and radial interface segregation results in the liquid after 2000s of growth at 3.34 $\mu\text{m/s}$, with 1500s of growth at constant $1\mu\text{g}$, the next 500s of growth with g-jitter added. The direction U is along the length of the sample, V is parallel to the interface.

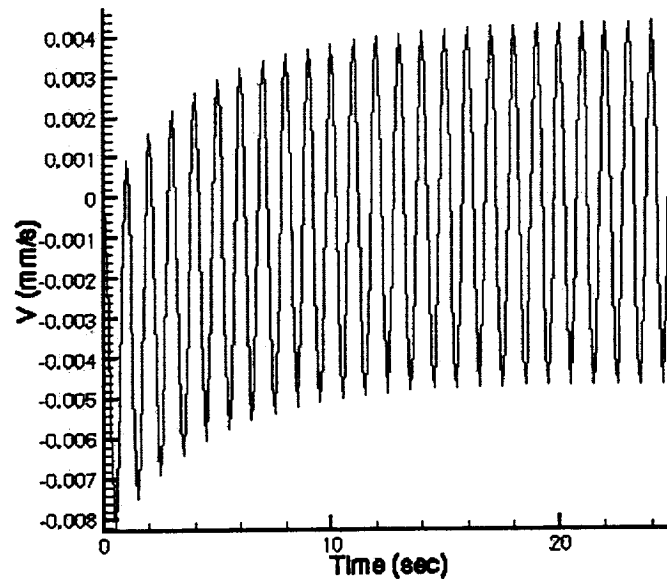


(a)



(b)

Figure 3. Vertical velocity at the reference point for an amplitude of $10^{-3}g$ and frequencies of (a) 10^{-2} Hz, (b) 10^{-1} Hz and (c) 1 Hz.



(c)

Figure 3. Vertical velocity at the reference point for an amplitude of $10^{-3}g$ and frequencies of (a) 10^{-2} Hz, (b) 10^{-1} Hz and (c) 1 Hz.

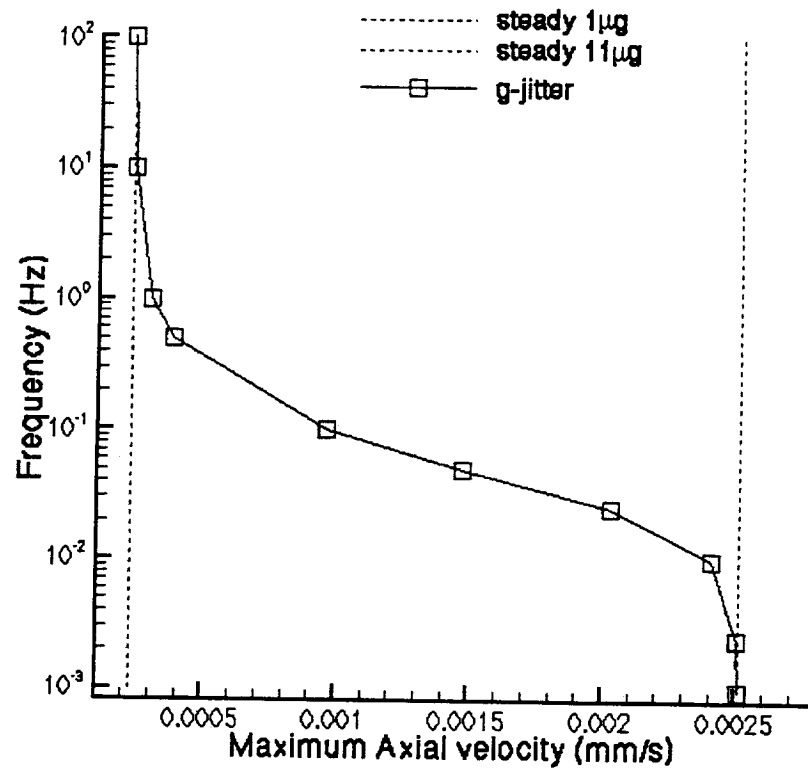


Figure 4 The relation between maximum axial velocity and frequency of the disturbance.

Background gravity ($1\mu\text{g}$)

Peak of the gravity ($11\mu\text{g}$)

convectively carry the solute away from the interface. As a result, the concentration near the interface is decreased after one cycle of the disturbance. Because the acceleration changes slowly, the velocity field has enough time to change with it; and since flow velocities are high the transport of solute is dominated by the flow. As seen in the animation, oscillations in velocity and concentration are almost in phase. For this case longitudinal segregation is expected to be high due to solute transport to the far field liquid.

Movie 5 shows the effects of the disturbance of 0.05Hz and $10^{-2}g$. In this case, the solute profile established during steady $1 \mu g$ conditions is significantly modified when g-jitter starts with the decrease of concentration in the mid-height. As a result, the highest amount of radial segregation at the interface was observed in this case (see Table 4). Far field mixing of solute appears to be less in this case as compared to Movie 4, thus longitudinal segregation is expected to be less.

Movie 6 shows the effects of the disturbance of 0.1Hz and $10^{-2}g$. In the previous 2 cases, the flow was swift enough to sweep the solute across the interface with higher concentrations resulting in the corners where velocities are restricted. For this case, the moderate flow only has enough time and strength to sweep the solute about half way across the interface before reversing; thus resulting in the highest concentrations being located near the centreline and a reversal in radial segregation as compared to Movies 4 and 5, as seen in the animation. In this case, a small time delay between concentration field and velocity field is observed.

Movie 7 shows the effects of the disturbance of 1.0Hz and $10^{-2}g$. From the animation, it can be seen that even though the amplitude is high its effect on the solute field is relatively small due to the higher frequency. Though the solute field is still significantly corrupted from the pure diffusion case as seen in the radial segregation. (Table 4).

Movie 8 shows the effects of the disturbance of 0.01Hz and $10^{-3}g$. In this case, the frequency is the same as that in Movie 4. However, the amplitude of the disturbance is smaller ($10^{-3}g$). Therefore, the convection is not strong enough to mix the solute much with the far field liquid (at this growth rate). However, the velocity field is still strong enough to induce radial solute variations, as seen in the animation and in Table 4.

Movie 9 shows the effects of the disturbance of 0.1Hz and $10^{-3}g$. From the animation, little if any effect on solute due to g-jitter can be seen; however, Table 3 does show radial segregation caused by the g-jitter.

Average Concentration at the interface

Figure 5 shows the solute concentration distribution at the mid-height of the sample at the start of g-jitter and after a further 500 seconds of solidification for the oscillation frequencies of 0.01, 0.1 and 1 Hz, with an amplitude of $10^{-3}g$ and also for a steady gravitational acceleration.

At the time g-jitter starts, 5 mm of the sample had been solidified, creating a solute rich boundary layer in front of the interface. The peak value of concentration in the liquid at the interface caused by solute rejection into the liquid reached almost 7 at%. The solute concentrations in the liquid at the interface decay exponentially with the distance away from the interface to a value of C_0 .

After another 500 seconds of solidification the maximum concentration at the mid-height of the ampoule reached 8.33 at% for the steady gravitational acceleration, 8.43 at% and 8.38 at% for frequencies of 0.1 and 1Hz, and 7.26 at% for 0.01 Hz. The largest difference in the maximum value (12.8%) occurs at the lowest frequency of 0.01 Hz. In this case convection has developed, resulting in the redistribution of solute in the melt and hence at the interface. The difference between the low 0.01 Hz frequency and the other cases can clearly be observed in Figure 6 which shows the history of the average concentration at the interface during 500 seconds of solidification. Even though longitudinal segregation in the 0.1 Hz case is nearly the same as the pure diffusion case, Table 4 and Figure 7 show significant radial segregation at the $10^{-3}g$, 0.1 Hz condition; thus this case is not resulting in diffusion controlled growth.

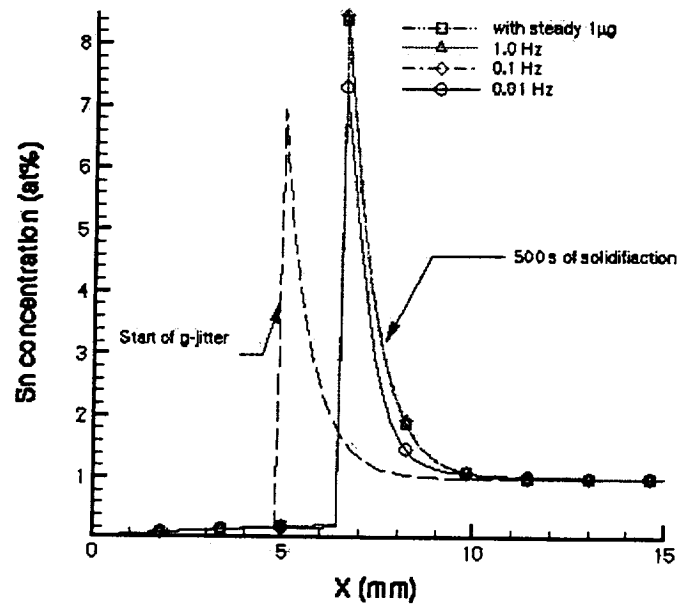


Figure 5. Distribution of solute concentration at the mid-height of the ampoule after 500 seconds of solidification with a g-jitter amplitude of $10^{-3}g$.

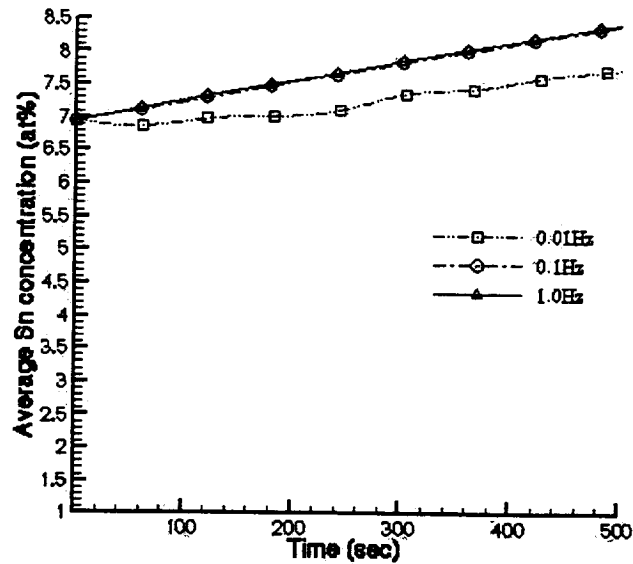


Figure 6. Average liquid interface concentration during growth with g-jitter of $10^{-3}g$ at frequencies of 10^{-2} , 10^{-1} and 1 Hz. Starting time is after 1500s of growth without g-jitter.

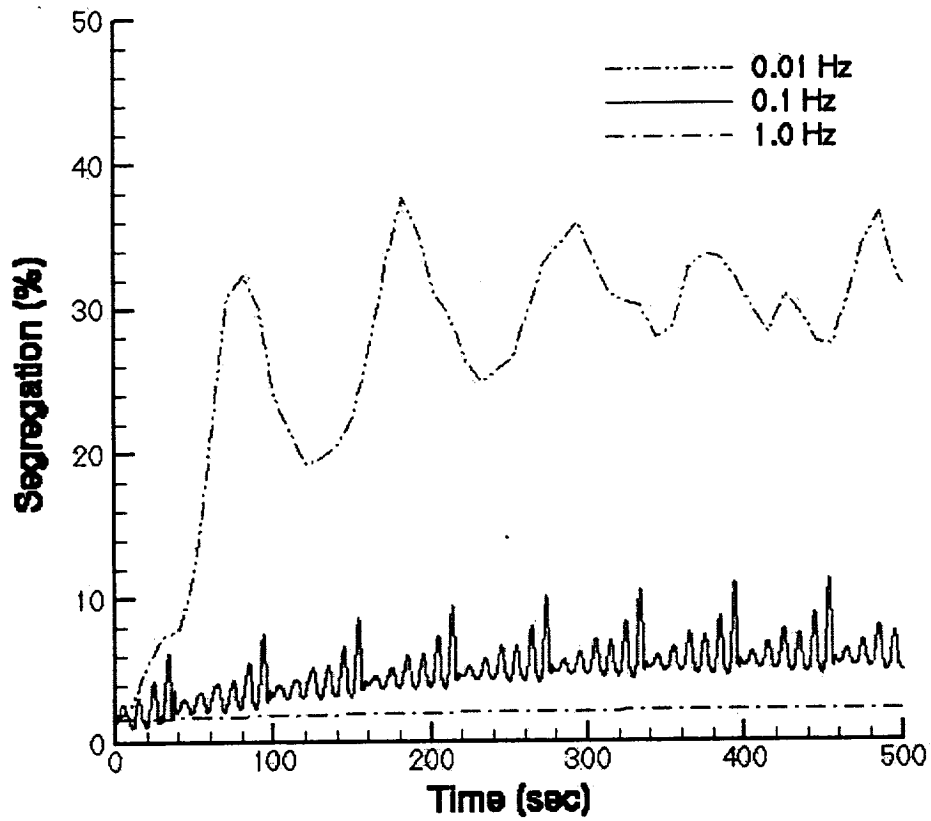


Figure 7. Radial segregation in the liquid at the interface during growth with g-jitter of amplitude of 10^{-3} g and frequencies of 10^{-2} , 10^{-1} and 1 Hz; showing growth at 1 Hz to be diffusion controlled and the solute profiles for the 10^{-2} and 10^{-1} Hz cases to be modified by convection.

The resulting radial segregation in the liquid at the interface can be seen in Figure 7. The segregation at the interface for the 0.1 and 0.01 Hz cases fluctuates with a frequency corresponding to that of the disturbances. The oscillations are real, however the different magnitude of the peaks in the case of the 0.1 Hz frequency and their periodic change are not real but rather an artefact of the fixed grid finite volume formulation which is used. In this formulation all the computed values are cell averaged values which are changing while the interface passes through one partially solidified cell.

Finally, disturbances with an amplitude of $10^{-2}g$ are considered. The time history of the average liquid concentration at the interface during 500 seconds of solidification with g-jitter (after 1500 seconds of solidification at constant $1 \mu g$) is shown in Figure 8. At 1 Hz the average interface concentration follows closely that expected during the initial transient for diffusion controlled growth (see Figure 6); thus indicating that far field mixing of the solute being produced at the interface is negligible. Growth for this case ($10^{-2}g$, 1 Hz) is not, however, dominated by diffusion, since the solute profiles near the interface are corrupted from the diffusion case as shown in the radial segregation results, Table 4. For the 0.1 Hz ($10^{-2}g$) case the departure of the average interface concentration from the diffusion case indicates significant mixing of solute from the neighbourhood of the interface with the far field liquid; radial segregation is also high (Table 4) with the maximum radial segregation occurring between (at $10^{-2}g$) 0.1 and 0.01 Hz. The decrease in radial segregation after the frequency is lowered from 0.05 to 0.01 Hz (at $10^{-2}g$) and interface concentration approaching C_0 (Figure 8) indicates that the solute is becoming well mixed with the far field liquid for the 0.01 Hz, $10^{-2}g$ case.

At 0.1 Hz, $10^{-2}g$ the flow at first carries low concentration solute from the bulk of the liquid closer to the interface, some mixing occurs in the liquid and as a result the average concentration at the interface decreases while the interface is moving through the liquid. However, once the flow starts to oscillate backwards and forward, and additional solidification occurs with solute rejection and mixing with the far field liquid, the average concentration levels out and is expected to rise as solidification continues. The radial segregation in this case reaches 39.9% after 500 seconds of g-jitter. At 0.01 Hz the average concentration drops quickly due to bulk mixing of solute. At 60 seconds the flow reverses and brings back high concentration solute causing an increase in the average concentration at the interface. As the magnitude of the velocity increases in the opposite direction, further mixing occurs in the liquid and the average concentration drops to about 1.5%.

A non-dimensional quantity of interest in this analysis is the solutal Peclet number, defined as $Pe_s = (V_j \delta) / D$, where V_j is the predominant flow velocity in the solute boundary layer, δ is the boundary layer thickness equal to $2D/R$, and R is the growth rate. In general, growth is considered to be diffusion dominated if $Pe_s < 1$. If we consider the vertical velocity maximum, V_{max} , to be characteristic of the flow inside the solute boundary layer, it can be seen from Table 4 that no signs of convection (radial segregation) are present for V_{max} values less than about 1×10^{-3} mm/s and that diffusion conditions are clearly departed from at V_{max} values greater than about 1×10^{-2} mm/s; these velocities correspond to Pe_s of between about 0.6 to 6.0 respectively, which is in excellent agreement with the stated general application of this non dimensional number. The Rayleigh numbers ($Ra = \frac{g \beta \Delta T h^3}{\nu \alpha}$) assuming constant $10^{-5}g$ and $10^{-4}g$, and thermally driven flow for these V_{max} values are 1.09 and 10.9 respectively. By scaling V_{max} to the Rayleigh number the consequences of changing the g level, furnace temperature gradient, ampoule diameter (h), and sample material can be estimated. With Pe_s the consequences of changing the growth velocity can also be estimated.

It is also noteworthy that the effects of solute on the fluid flow are not readily seen in these simulations because only about 6.7 mm of sample are solidified; thus simulations take place in the early stage of the initial transient. The result is that the solute boundary layer is not built up very high. With further solidification, additional solute would be rejected and possibly the creation of a solutally driven flow

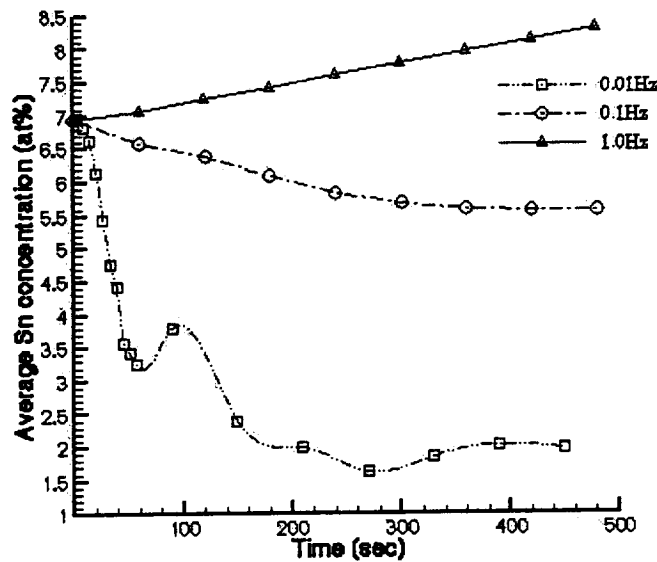


Figure 8. Average liquid concentration at the interface during growth with g-jitter of $10^{-2}g$ at frequencies of 10^{-2} , 10^{-1} and 1 Hz; showing no solute mixing with the far field liquid at 1 Hz, partial mixing at 10^{-1} Hz, and nearly complete mixing of the solute rejected at the interface with the far field liquid at 10^{-2} Hz.

cell (rather than the thermally driven cells found in this work). Previous work has shown the development of solutally driven cells.⁶

Temperature field and interface shape

Figure 9 and Figure 10 show the interface shape with time for the disturbance of 0.01 Hz with $10^{-2}g$ and $10^{-3}g$ respectively. It can be concluded that the interface shape is not flat when there is a strong convection. As seen in Figure 9, the interface shape develops corresponding to the flow inside the domain. However, for $10^{-3}g$ amplitude of disturbance, it is shown that (while assuming constant interface temperature) the flow field is not strong enough to change the shape of the interface (see Figure 10).

When considering Figures 9 and 10 it should be kept in mind that the S/L interface temperature has been assumed constant. Thus the effects of solutal gradients at the interface on the interface temperature have not been included. As seen in Table 4, the concentration in the liquid across the interface can vary by a factor of 2 or more. If, for example, we assume a concentration variation from 5 at% to 10 at% at the interface, these locations would vary in temperature by about $12^{\circ}C$ ($\Delta C(m) = (10-5\text{at\%}) \cdot 2.32^{\circ}C/\text{at\%}$). With an axial temperature gradient of $20^{\circ}C/\text{mm}$, these locations would vary axially by about 0.6 mm., which indicates much more interface curvature due to solute dependent interface temperature than that caused by the flow modifying the temperature field.

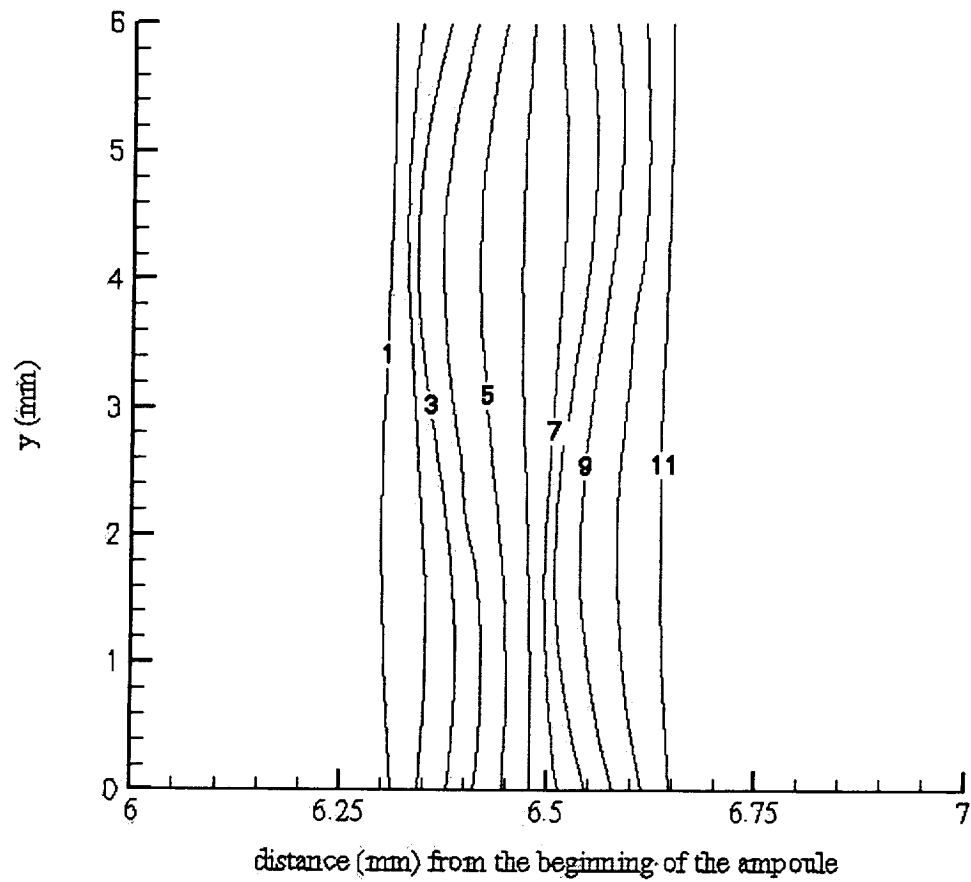


Figure 9. Isothermal interface shape for the disturbance of $10^{-2}g$ and 0.01 Hz from 400 - 500 sec (time interval 10 sec). Note that the horizontal and vertical scales are not the same; the curvature of the interface is exaggerated.

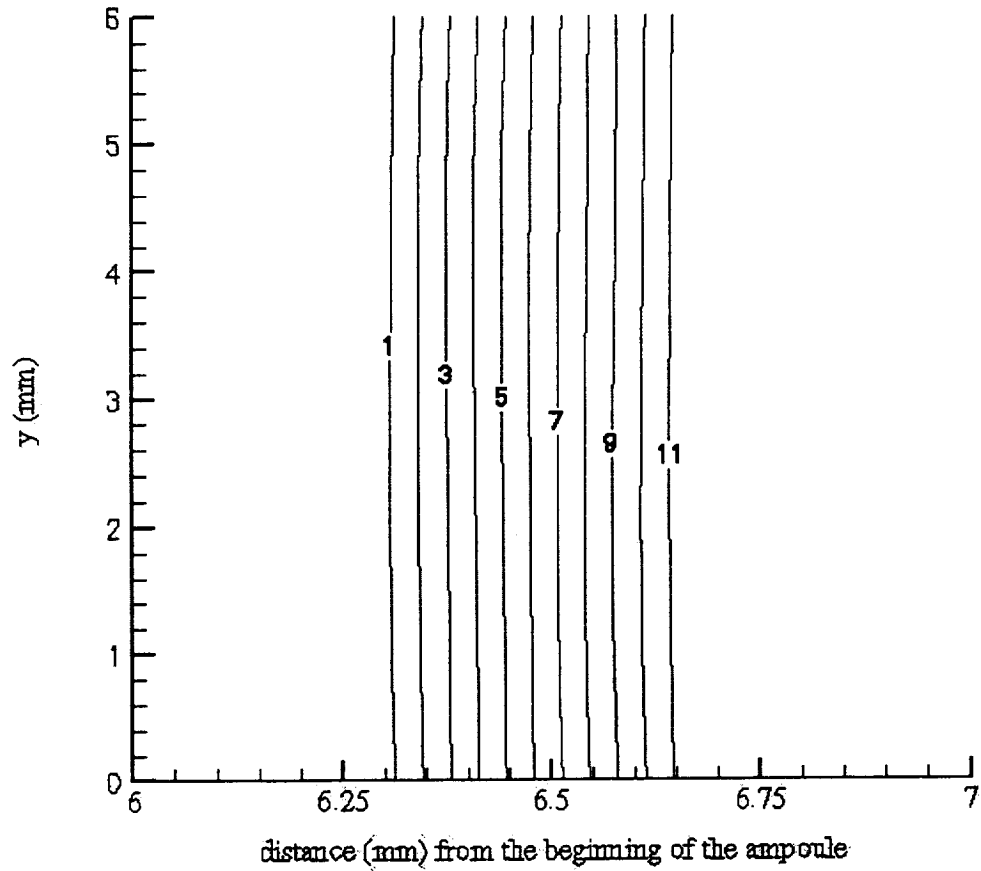


Figure 10. Isothermal interface shape for the disturbance of $10^{-3}g$ and 0.01 Hz from 400 - 500 sec (time interval 10 sec). This simulation does not include the influence of radial segregation and effect of solute on the temperature (and thus the shape) of the interface.

6. CONCLUSIONS

We have investigated numerically effects of sinusoidal disturbances with amplitudes from $10^{-5}g$ to $10^{-2}g$ and frequencies from 10^{-2} to 1 Hz on the solute redistribution and segregation at the interface during directional solidification of Bi-1at% Sn alloy.

It was found that for large frequencies a higher amplitude of the gravitational acceleration is required to produce an effect on the segregation. For example, disturbances with frequencies from 0.5 to 1 Hz and amplitudes less than $10^{-2}g$ produce very little effect on the segregation. For this frequency range an amplitude of $10^{-2}g$ resulted in 20.2% and 10.9% segregation compared with a segregation of 1.8% for the steady $1\ \mu g$ case. For frequencies from 0.05 Hz to 0.1 Hz, an amplitude of $10^{-3}g$ results in the segregation changing to 11.3% and 8.9% respectively. The largest effect on the segregation was produced by disturbances with a frequency of 0.01 Hz, where the maximum segregation was equal to 4.9% for an amplitude of $10^{-4}g$, 38.2% for an amplitude of $10^{-3}g$ and 188.7% for an amplitude of $10^{-2}g$. In the last case significant mixing of the solute in the cavity was observed. Diffusion dominated conditions were observed at solutal Peclet numbers below 0.6, convection was significant at $Pe_s > 6.0$. Rayleigh numbers below about 1.1 resulted in diffusion dominated growth at $R = 3.34\ \mu m/s$, at $Ra > 11.0$ corruption of diffusion conditions was observed (at the growth rate examined). Under the conditions examined in this work, the shape of the interface can not be accurately simulated if the influence of solute on interface melting temperature is omitted.

REFERENCES

1. Abbaschian, R., et al., *33rd Aerospace Sci. Meeting, AIAA 95-0608*, 1995.
2. Alexander, J.I.D., Ouazzani, J., Rosenberger, F., 1989, Analysis of the low gravity tolerance of Bridgman-Stockbarger crystal growth: I. Steady and impulse accelerations, *J. Crystal Growth*, Vol. 97, pp. 285-302.
3. Alexander, J.I.D., Amiroudine S., Ouazzani, J., Rosenberger, F., 1991, Analysis of the low gravity tolerance of Bridgman-Stockbarger crystal growth: II. Transient and periodic accelerations, *J. Crystal Growth*, Vol. 113, pp. 21-38.
4. Andrews, J.B., Hayes, L.J., Arikawa, Y., Coriell, S.R., *35th Aerospace Sci. Meeting, AIAA 97-1012*, 1997.
5. Cambon, G., et al., *49th Int. Astro. Cong., IAF/IAA-98-J.3.04*, 1998.
6. de Groh III, H.C. and Nelson, E.S., 1994, Heat Transfer in Micro-g Systems, *ASME-HTD*, Vol. 290, 23.
7. DeLombard, R., "Compendium of information for interpreting the microgravity Environment of the Orbiter spacecraft," NASA TM 107032, 1996.
8. Fripp, A.L., Debnam, W.J., Woodell, G.A., Rosch, W.R., Narayanan, R., *35th Aerospace Sci. Meeting, AIAA 97-0676*, 1997.
9. Garandet G.P., Corre S., Favier J.J. and Alexander, J.I.D., On the effect of gravity perturbations on composition profiles during Bridgman crystal growth in space, *J. Crystal Growth*, Vol. 165, pp. 471-481, 1996.
10. Matthiesen, D.H. and Majewski, J.A., *NASA Conference Publ. 3272*, 1, 223, 1994.
11. Morgan, K., Lewis, R.W. and Zienkiewicz, O.C., 1978, An improved algorithm for heat conduction problems with phase change, *Int. J. Numer. Meth. Eng.*, Vol. 12, pp. 1191-1195.
12. Nelson, E.S., "An examination of anticipated g-jitter on Space Station and its effects on materials processes," NASA TM 103775, 1991.
13. Rogers, M., "Summary report of mission acceleration measurements for STS-87, launched Nov. 19, 1997," NASA TM-1999-208647, 1999.
14. Timchenko, V., Chen, P.Y.P., de Vahl Davis, G. and Leonardi, E., 1998, 'Directional Solidification in Microgravity', *Heat Transfer 1998*, J.S. Lee (ed), Taylor & Francis, pp. 241-246.
15. Voller, V.R., Brent, A.D. and Prakash, C., 1989, The modeling of heat, mass and solute transport in solidification systems, *Int. J. Heat Mass Transfer*, Vol. 32, pp 1719-1731.
16. Wilcox, W.R. and Papazian, J.M., 1978, *AIAA J.*, vol. 16, pp. 447.

REPORT DOCUMENTATION PAGE			Form Approved OMB No. 0704-0188	
<small>Public reporting burden for this collection of information is estimated to average 1 hour per response, including the time for reviewing instructions, searching existing data sources, gathering and maintaining the data needed, and completing and reviewing the collection of information. Send comments regarding this burden estimate or any other aspect of this collection of information, including suggestions for reducing this burden, to Washington Headquarters Services, Directorate for Information Operations and Reports, 1215 Jefferson Davis Highway, Suite 1204, Arlington, VA 22202-4302, and to the Office of Management and Budget, Paperwork Reduction Project (0704-0188), Washington, DC 20503.</small>				
1. AGENCY USE ONLY (Leave blank)		2. REPORT DATE April 2000		3. REPORT TYPE AND DATES COVERED Technical Memorandum
4. TITLE AND SUBTITLE Effects of Space Environment on Flow and Concentration During Directional Solidification				5. FUNDING NUMBERS WU-101-43-0B-00
6. AUTHOR(S) C. Benjapiyaporn, V. Timchenko, E. Leonardi, G. de Vahl Davis, and H.C. de Groh III				
7. PERFORMING ORGANIZATION NAME(S) AND ADDRESS(ES) National Aeronautics and Space Administration John H. Glenn Research Center at Lewis Field Cleveland, Ohio 44135-3191				8. PERFORMING ORGANIZATION REPORT NUMBER E-11767
9. SPONSORING/MONITORING AGENCY NAME(S) AND ADDRESS(ES) National Aeronautics and Space Administration Washington, DC 20546-0001				10. SPONSORING/MONITORING AGENCY REPORT NUMBER NASA TM-2000-209293
11. SUPPLEMENTARY NOTES C. Benjapiyaporn, V. Timchenko, E. Leonardi and G. de Vahl Davis, The University of New South Wales, Sydney NSW, Australia; and H.C. de Groh III, NASA Glenn Research Center. Responsible person, H.C. de Groh III, organization code 6712, (216) 433-5025. This report complete with movies is available online: ftp://ftp-gltrs.grc.nasa.gov/GLTRS/reports/2000/TM-2000-209293/index.html				
12a. DISTRIBUTION/AVAILABILITY STATEMENT Unclassified - Unlimited Subject Categories: 26, 29, and 34 Available electronically at http://gltrs.grc.nasa.gov/GLTRS This publication is available from the NASA Center for AeroSpace Information, 301-621-0390.				12b. DISTRIBUTION CODE
13. ABSTRACT (Maximum 200 words) A study of directional solidification of a weak binary alloy (specifically, Bi - 1 at% Sn) based on the fixed grid single domain approach is being undertaken. The enthalpy method is used to solve for the temperature field over the computational domain including both the solid and liquid phases; latent heat evolution is treated with the aid of an effective specific heat coefficient. A source term accounting for the release of solute into the liquid during solidification has been incorporated into the solute transport equation. The vorticity-stream function formulation is used to describe thermo-solutal convection in the liquid region. In this paper we numerically investigate the effects of g-jitter on directional solidification. A background gravity of 1 µg has been assumed, and new results for the effects of periodic disturbances over a range of amplitudes and frequencies on solute field and segregation have been presented.				
14. SUBJECT TERMS Gravity; Acceleration; Space experiment; Microgravity				15. NUMBER OF PAGES 30
				16. PRICE CODE A03
17. SECURITY CLASSIFICATION OF REPORT Unclassified	18. SECURITY CLASSIFICATION OF THIS PAGE Unclassified	19. SECURITY CLASSIFICATION OF ABSTRACT Unclassified	20. LIMITATION OF ABSTRACT	